This is a preprint, the final version is subject to change, of the American Mineralogist (MSA)
Cite as Authors (Year) Title. American Mineralogist, in press.
(DOI will not work until issue is live.) DOI: http://dx.doi.org/10.2138/am-2016-5458

1 **Revision 3**

2 High-temperature and high-pressure behavior of carbonates in the 3 ternary diagram $CaCO_3$-$MgCO_3$-$FeCO_3$

4

5 Marco Merlini[1,*], Francesca Sapelli[1], Patrizia Fumagalli[1], G. Diego Gatta[1], Paolo Lotti[1], Simone Tumiati[1],

6 Mahmoud Abdellatief [2], Andrea Lausi[2], Jasper Plaisier[2],

7 Michael Hanfland[3], Wilson Crichton[3], Julien Chantel[3,†], Jeremy Guignard[3,‡],

8 Carlo Meneghini[4],

9 Alessandro Pavese[1], Stefano Poli[1]

10 [1] Università degli Studi di Milano, Dipartimento di Scienze della Terra, Via Botticelli, 23, 20133 Milano,
11 Italy

12 [2] Sincrotrone Trieste, ELETTRA, Basovizza, TS, Italy

13 [3] European Synchrotron Radiation Facility, 6 Rue Jules Horowitz, 38043 Grenoble Cedex, France

14 [4] Dipartimento di Scienze, Università Degli Studi Roma TRE, Rome, Italy

15 *corresponding author: marco.merlini@unimi.it

16 [†]now at: Department of Earth, Environmental, and Planetary Sciences, Case Western Reserve University,
17 Cleveland, Ohio 44106 (U.S.A.)

18 [‡]now at: Université de Toulouse,Toulouse, France

19

20

Abstract

We report the thermal expansion and the compressibility of carbonates in the ternary compositional diagram $CaCO_3$-$MgCO_3$-$FeCO_3$, determined by *in-situ* X-ray powder and single-crystal diffraction. High-temperature experiments were performed by high-resolution X-ray synchrotron powder diffraction from ambient to decarbonation temperatures (25-850 °C). Single-crystal synchrotron X-ray diffraction experiments were performed in a variable pressure range (0-100 GPa), depending on the stability field of the rhombohedral structure at ambient temperature, which is a function of the carbonate composition. The thermal expansion increases from calcite, $CaCO_3$, α_0=4.10(7) *10^{-5} K^{-1}, to magnesite, $MgCO_3$, α_0=7.04(2)*10^{-5} K^{-1}. In the magnesite-siderite ($FeCO_3$) join, the thermal expansion decreases as iron content increases, with an experimental value of α_0=6.44(4)*10^{-5} K^{-1} for siderite. The compressibility in the ternary join is higher (*i.e.*, lower bulk modulus) in calcite and Mg-calcite [K_0=77(3) GPa for $Ca_{0.91}Mg_{0.06}Fe_{0.03}(CO_3)$] than in magnesite, K_0=113(1) GPa, and siderite, K_0=125(1) GPa. The analysis of thermal expansion and compressibility variation in calcite-magnesite and calcite-iron-magnesite joins clearly shows that the structural changes associated to the order-disorder transitions (*i.e.*, *R*-3*c* calcite-type structure *vs.* *R*-3 $CaMg(CO_3)_2$ dolomite-type structure) do not affect significantly the thermal expansion and compressibility of carbonate. On the contrary, the chemical compositions of carbonates play a major role on their thermo-elastic properties. Finally, we use our *P-V-T* equation of state data to calculate the unit-cell volume of a natural ternary carbonate, and we compare the calculated volumes to experimental observations, measured *in situ* at elevated pressure and temperatures, using a multianvil device. The experimental and calculated data are in good agreement demonstrating that the equation of state here reported can describe the volume behavior with the accuracy needed, for example, for a direct chemical estimation of carbonates based on experimental unit-cell volume data of carbonates at high pressures and temperatures.

Introduction

The interest in carbonate mineralogy has grown significantly in the last decades. These minerals can in fact provide clues and information about recent and past Earth's climate history. Carbonates are involved in fundamental geological processes related to the global carbon cycle. In particular, a shallow carbon cycle (*i.e.*, involving exchanges between atmosphere and hydrosphere reservoirs) is directly related to the dissolution and precipitation of carbonates, mainly calcite, in the oceans. The carbonate-bearing sediments are involved also in subduction processes. The stability of carbonate in these environments is the key issue to understand the transfer of crustal carbon into the inner Earth or its recycling through volcanism. Carbon is also stored in the Earth's mantle in various forms, as demonstrated by natural occurrence of diamonds. Some of these diamonds also present carbonate, or CO_2 as inclusions (*e.g.*, Berg, 1986, Navon, 1999). It is now clear that a thermodynamic modelling of carbonate stability in various environments is fundamental for a deeper understanding of global carbon cycle. Thermodynamic data on the ternary composition diagram calcite-magnesite-siderite are scarce, especially for iron-bearing carbonates. A direct experimental observation of the stable composition as function of pressure, temperature and chemical composition is probably the most successful approach for a detailed understanding of carbonate stability. In recent years, the availability of large-volume high-pressure devices at synchrotron sources has allowed a number of possible experiments to be performed. The accuracy in diffraction and pressure-temperature control can nowadays provide reliable crystallographic information at given *P* and *T* conditions. While planning a series of experiments, we realized that literature data about *P*-*V*-*T* equations of state (EoS) of carbonate are not only scarce, but also contradictory. This is especially evident for thermal properties, especially in iron-bearing members. The knowledge of accurate EoS is necessary in order to properly extract chemical information from *in-situ* experiments, where the most direct information on these phases is their unit-cell volume and edges lengths. To fix the discrepancies in *P*-*V* and *V*-*T* data and fill the gap for missing compositions, we performed new high-temperature and high-pressure experiments on well-characterized samples.

We report, in the current paper, the results of high-resolution X-ray powder diffraction measurements at high temperature and single-crystal experiments at high pressure. The *V*-*T* and *P*-*V* equations of state are finally compared with *in-situ* experiments at simultaneously high pressure and high temperature.

Materials and methods

Natural and synthetic samples were used in this study. Table 1 reports the samples, their provenance and chemical composition. The chemical analyses were performed with a Jeol Superprobe instrument available at the Earth Sciences Department, University of Milan, Italy (ESD-Mi). The calibration of the instrument was performed with standard mineral samples.

Single-crystal diffraction at ambient conditions was performed with the Oxford Diffraction X'Calibur diffractometer, equipped with Mo-*K*α source and CCD detector, at ESD-Mi. We used standard operating conditions for data collection, performing 0.75° ω-axis scans (Busing and Levy 1967) at variable φ, κ and θ axis configurations. The raw data were integrated with the Crysalis Red software (Oxford Diffraction 2008) and structure refinements were performed with the Jana2006 program (Petricek et al. 2014).

Three samples were synthesized with the end-loaded piston cylinder at ESD-Mi. We employed the standard procedures commonly in use for double stage piston cylinders. The starting material was a mixture of carbonates (calcite:dolomite 5:95%; calcite:Fe-dolomite 80:20%). The samples were finely grounded in ethanol to assure a homogeneous mixing. The starting material was inserted in a welded Pt capsule, and before welding, a tiny amount of water (apx. 2%) was added, to promote growth of homogeneous crystals. The synthesis experiments were run at 2.0 GPa and 1050 °C for 2 days. The synthesis ended up with crystals with variable size, up to 100x100x100 μm^3.

The X-ray high-temperature (room-pressure) powder diffraction experiments were performed at the MCX beamline at the Elettra synchrotron facility (Trieste, Italy), the beamline being described in Rebuffi et al. (2014). The X-ray diffraction patterns were collected with the high-resolution two circle diffractometer available at the beamline. A monochromatic beam of 0.8270 Å was used, and diffraction patterns were collected over the angular range of 10-30 ° 2θ, with a 0.0075° step size. High-temperature conditions were maintained with a hot gas blower. The sample temperature was monitored by the use of quartz as internal standard in five different experiments. The comparison of unit-cell parameters with reference data (Kihara 1990) and the alpha/beta quartz transition demonstrates that the temperature is accurate within 1-2 °C and perfectly reproducible in the different runs (Deposit Items). To avoid any possible reaction between the

carbonate and quartz, the quartz powder was inserted in a 0.2 mm quartz capillary, within the larger (0.7mm) capillary containing the sample. The diffraction patterns were analyzed by the Rietveld method, using the GSAS+EXPGUI software (Larson et al. 1994; Toby 2001). Two additional measurements were performed in a CO_2 atmosphere using the furnace operating under controlled atmosphere (Riello et al. 2012) equipped with an imaging plate detector.

The X-ray high-pressure (room-temperature) single-crystal diffraction experiments were performed at the ID09A beamline (ESRF, Grenoble, France) with the standard beamline setup (Merlini and Hanfland 2013). We used a monochromatic radiation having wavelength λ=0.41414 Å. The diffraction spots were collected with the Mar555 flat panel detector, at a distance of 300 mm from the sample, and images were recorded while integrating over 1° step size during an ω-rotation (Busing and Levy 1967). High-pressure conditions were generated with a membrane-type diamond anvil cell (DAC) using diamonds with Boheler-Almax cut and variable culet size (600, 300, 125 μm diameter), depending on the target pressure. The gaskets were made with a rhenium foil and the *P*-transmitting medium was helium or neon. The pressure was determined by the ruby-fluorescence method (Forman et al. 1972; Mao et al. 1986) or with Sm:borate (Datchi et al. 1997) for the Mbar experiment. The raw data were integrated with the Crysalis Red program and single-crystal structural refinements were performed with Jana2006 software.

The high-pressure/high-temperature experiments were performed at the ID06 beamline at the ESRF, using the high-resolution setup. High-pressure conditions were generated by a 20MN large-volume device. The experiments were performed using a standard 10/4 mm multi-anvil assembly, with pyrophyllite gaskets and sample directly contained within the graphite furnace. Co-axial to the incident beam direction, a boron:epoxy rod was inserted to avoid X-ray diffraction signal from the spinel and MgO from the Cr-doped octahedron. A 'C'-type thermocouple was included in the assembly for temperature measurements. Pressures and temperatures during the experiments were calculated with cross matching of thermocouple values, heating power, thermal EoS of graphite (Hanfland et al. 1989; Colonna et al. 2011) and MgO (Hazen 1976; Dewaele et al. 2000). Pressure was increased up to 3 GPa at room-*T*, and then the temperature was increased. Monochromatic X-ray diffraction patterns (λ=0.3757 Å) were collected with a Tl:NaI Bicron scintillator detector, scanning on a large-radius (~1350 mm) pseudorotation over the 2θ angular range of 5-25°, with

step size 0.001°. Two sets of adjustable slits were used to define the volume of the diffracting sample, and thus shield diffraction signal from the up- and downstream pyrophyllite gaskets and the furnace. Angular calibration of the instrument was performed before the experiment against NIST standard LaB_6 SRM660a. The data were analyzed by the Rietveld method, using the GSAS+EXPGUI software (Larson et al. 1994; Toby 2001).

Results

- Crystal structure of synthetic and natural samples by single-crystal X-ray diffraction

Fourteen different carbonates (Table 1) were investigated by single-crystal X-ray diffraction, to characterize the samples used for thermal expansion and compressibility measurements.

All the samples crystallize in calcite-type structure (*R*-3*c*) except dolomite and Fe-dolomite samples (*R*-3). All the structural details are reported in Table 1 and in the Deposit Items.

We may consider different binary compositional joins, in particular the calcite-magnesite; calcite-Fe-magnesite; dolomite-ankerite and magnesite-siderite. The unit-cell edges and volume vary almost linearly in the four different binary joins considered, and are independent from the symmetry of the sample. These results are summarized in Fig. 1. The variation of the unit-cell parameters in the ternary compositional carbonate system, at a first approximation, can be described with the following simple equations involving the concentration of $CaCO_3$, $MgCO_3$ and $FeCO_3$:

$$a\ (\text{Å}) = 4.985\ X_{CaCO3} + 4.636\ X_{MgCO3} + 4.696\ X_{FeCO3}$$

$$c\ (\text{Å}) = 17.064\ X_{CaCO3} + 15.033\ X_{MgCO3} + 15.414\ X_{FeCO3}$$

$$Vol\ (\text{Å}^3) = 366.2\ X_{CaCO3} + 279.2\ X_{MgCO3} + 294.1\ X_{FeCO3}$$

The numerical values are derived from a fit on the experimental data. X_{CaCO3}, X_{MgCO3}, X_{FeCO3} are, respectively, the molar fraction of the calcitic, magnesitic and sideritic components in the considered carbonate. The data agree with literature data (*e.g.*, Effenberger et al. 1981; Reeder and Dollase 1989; Boulard et al. 2012).

A comprehensive discussion on the chemical effects on structural parameters is widely discussed in the literature (*e.g.*, Effenberger et al. 1981; Reeder 1983; Reeder and Dollase 1989; Redfern 2000). The *R*-3 double-carbonates analyzed (dolomite and Fe-dolomite) present a fully ordered cation distribution (Ca and

Mg+Fe, respectively) over the two cation sites. The synthetic Mg-calcite samples possess the calcite-type structure (*R*-3*c*) and no evidence of partial ordering is detected by X-rays, within the experimental accuracy. The synthetic sample $Ca_{0.55}Mg_{0.45}(CO_3)$ has also a calcite-type structure, *R*-3*c*, as demonstrated by structure refinement (Deposit Items). This indicates that a slight Ca excess in dolomite may quench as a fully disordered dolomite structure.

- Thermal expansion: synchrotron X-ray powder diffraction experiments

Powdered samples from the batch crystals described in the previous section were used for the high-temperature thermal expansion measurements. Fig. 2 shows an example of an X-ray powder pattern containing calcite and quartz as internal standard. The Full Width at Half Maximum (FWHM) of the diffraction peaks, over the angular range considered, is, on average, 0.03°. All the samples are analyzed by the Rietveld method, which allows the refinement of the unit-cell parameters at variable temperature (Deposit Items).

Calcite presents a negative thermal expansion along the *a*-crystallographic axis (Rao et al. 1968). The expansion parallel to the *c*-axis is positive, like the volume expansion. All the other samples analyzed present a positive expansion along both crystallographic directions except the Mg-Fe-calcite, which has an anomalous thermal behavior parallel to the crystallographic *a* axis, but significantly smoothed compared to pure calcite. This indicate that a minor incorporation of Mg and Fe may affect significantly the thermal behavior. The volume data are fitted with the formalism proposed by Pawley et al. (1996) and Fei (1995) commonly used in mineralogy and petrology (*e.g.*, Holland and Powell 1998; 2011; Angel et al. 2014).

Thermal expansion, defined as:

$$\alpha(T) = \frac{1}{V} * \frac{\partial V}{\partial T} \quad (1)$$

and can be described with a polynomial expression, for example (Pawley et al. 1996):

179 $$\alpha(T) = a_0 + \frac{a_1}{\sqrt{T}} \quad (2)$$

180 The equation resulting from integration of (1) using the expression (2) is:

181 $$V = V_0 * exp\,[a_0 * (T - T_0) + 2 * a_1 * (\sqrt{T} - \sqrt{T_0})\,] \quad (3)$$

182 which can be further simplified, by a Taylor expansion to:

183 $$V = V_0 * \left[1 + a_0 * (T - T_0) + 2 * a_1 * \left(\sqrt{T} - \sqrt{T_0}\right)\right] \quad (4)$$

184 A further simplification results from the empirical observation that for most materials, a_0 and a_1 are
185 correlated such that $a_1 \approx -10a_0$ (Pawley et al. 1996) leading to:

186 $$V = V_0 * \left[1 + a_0 * (T - T_0) - 20 * a_0 * \left(\sqrt{T} - \sqrt{T_0}\right)\right] \quad (5)$$

187 For comparison, we also used the formalism proposed by Fei (1995), in which the thermal expansion is
188 expressed as follows:

189 $$\alpha(T) = a_0 + a_1 * T \quad (6)$$

190 It results in the expression:

191 $$V = V_0 * exp\,[a_0 * (T - T_0) + 0.5 * a_1 * (T^2 - T_0^2)] \quad (7)$$

192 The experimental data were fitted with the expression (2) and (6) for the thermal expansion and the results
193 are reported in Table 2.

194

195 In the magnesite-siderite binary join, the thermal expansion coefficient decreases from the magnesite to the
196 siderite end-member (Fig. 3), and the variation is linear, as a first approximation. The current data provide a
197 clear indication on the degree of the effect of increasing Fe in magnesite, consisting of a sensible decrease of
198 the thermal expansion. In the dolomite-ankerite join, the rate of decrease of thermal expansion as a function

of Fe content is reduced, but Fe-dolomite still presents a lower expansion if compared to pure dolomite. The thermal expansion of dolomite is comparable to literature data (Markgraf and Reeder, 1986).

The effect of calcium on thermal expansion can be evaluated in the calcite-magnesite and calcite-Fe-magnesite compositional joins (Fig. 4). Calcite has the lowest expansion. A small incorporation of Mg and Fe in calcites drives the expansion values close to the ones of dolomite and Fe-dolomite. The calcite-Fe-magnesite join (after deriving the value for $Mg_{0.6}Fe_{0.4}CO_3$ from a linear fit on the magnesite-siderite mixture) indicates, further, that there is no evident effect of the actual symmetry (*R*-3*c* *vs.* *R*-3) on the thermal expansion of carbonates, which seems mostly determined by their composition.

All the samples here analyzed show an incipient decomposition at temperatures higher than 550-650 °C. In order to extend the experimental temperature range, a few measurements were performed under controlled atmosphere (P_{CO2} = 2 bar) and with a fast detector. Pure calcite undergoes two high temperature transitions, above 500 °C and 1000 °C respectively, to the $CaCO_3$-IV (*R*-3*c*) and $CaCO_3$-V (*R*-3*m*) polymorphs. These transitions are marked by a change in elasticity and symmetry, in agreement with previous observation (Mirwald 1976; Dove and Powell 1989; Redfern et al. 1989; Dove et al. 2005; Antao et al. 2009; Ishizawa et al. 2013). A detailed description of high temperature polymorphism is to be reported elsewhere. Dolomite-ankerite and magnesite-siderite do not extend their stability significantly, and decarbonation is detected above 650 °C. Mg-Fe-calcite has an enlarged stability domain, persisting as a single *R*-3*c* phase up to 800 °C. Above this temperature, a decomposition into $CaCO_3$, Fe_3O_4 and MgO is observed.

- Compressibility: synchrotron single crystal and powder X-ray diffraction experiments

Single-crystal high-pressure diffraction experiments were performed on nine different samples in the ternary compositional diagram (Table 3). The maximum pressure investigated depends on the stability field of rhombohedral carbonates (at ambient temperature). The experimental volume data are fitted with the formalism of the Birch-Murnagham (BM) Equation of State (EoS), truncated to the third order:

$$P = 1.5Ko * \left[\left(\frac{V}{V_0}\right)^{-\frac{7}{3}} - \left(\frac{V}{V_0}\right)^{-\frac{5}{3}}\right] * \left[1 + \frac{3}{4}(K' - 4) * \left(\left(\frac{V}{V_0}\right)^{-\frac{2}{3}} - 1\right)\right]$$

where K_0 is the isothermal bulk modulus and K' its pressure derivative.

Pure calcite is stable in rhombohedral *R*-3*c* symmetry up to a maximum pressure of 1.7 GPa (Merrill and Bassett 1975) at ambient temperatures, and was not analyzed further in this study. Single-crystal data for calcite at high pressure are reported in Redfern and Angel (1999). Dolomite and ankerite are stable in rhombohedral symmetry up to 15-20 GPa (Santillan et al. 2006; Mao et al. 2011; Merlini et al. 2012), with a transition pressure that is a function of composition and degree of order (Zucchini et al. 2014). Magnesite and siderite (Fiquet et al. 2002; Merlini and Hanfland 2013) are observed in rhombohedral symmetry above the Mbar. Iron, in rhombohedral carbonate, undergoes a high- to low-spin state transition above 45 GPa (Mattila et al. 2007; Lavina et al. 2010a; Lin et al. 2012). This electronic transition induces a volume collapse easily detectable by X-ray diffraction experiments, even when Fe is present as minor element (Lavina et al. 2012; Lin et al. 2012).

We performed high-pressure experiments on calcite and Mg-Fe-calcite samples and observed the calcite to calcite-II transition at 1.7 GPa for pure calcite, at similar pressure for $(Ca_{0.96}Mg_{0.02}Fe_{0.02})CO_3$ and at 2.5 GPa for $(Ca_{0.91}Mg_{0.06}Fe_{0.03})CO_3$. We collected enough data points for the determination of the equation of state of

243 $(Ca_{0.91}Mg_{0.06}Fe_{0.03})CO_3$. The evolution of the Eulerian finite strain (*f*) as function of the normalized pressure
244 (*F*), the *f-F* plot (Angel 2000), for this sample is consistent with an extremely low pressure derivative of bulk
245 modulus (Deposit Item) and a fit to a 3rd order BM-EoS results in a bulk modulus K_0=77(3) GPa with
246 negative *K'* = -4(1). This anomaly is probably related to the structural behavior, which rapidly proceeds to
247 the second-order transition of calcite to calcite-II structure. Such uncommon elastic anomalies, resulting in a
248 negative *K'*, are sometimes observed and it is the case, for example, of cordierite (Miletich et al. 2014). A fit
249 with a 2nd order BM EoS results in K_0= 65(1) GPa, significantly lower than pure calcite, as determined by
250 Redfern and Angel (1999), *i.e.*, K_0=73.5(3) GPa.

251 The compressibilities were determined for three samples close to dolomite-ankerite compositions. Pure
252 dolomite presents the dolomite to dolomite-II transition at 14 GPa, in agreement with recent results obtained
253 by Zucchini et al. (2014). The *f-F* plot (Angel 2000) for this sample (Deposit Items), indicates that a 2nd order
254 BM EoS is appropriate to describe the elastic behavior. The bulk modulus, 94(1) GPa, is similar to the
255 reported data and also to Ross and Reeder (1992). A sample close to dolomite in its disordered form,
256 $(Ca_{0.55}Mg_{0.45})CO_3$, has a quenched high-temperature disordered cation configuration. The *f-F* plot indicates
257 that for this sample the pressure derivative of bulk modulus is not 4, and a 3rd order BM should be used. The
258 refined values are K_0 = 89(2) GPa and *K'* = 3.0(2). The *K'* value lower than 4 may also relate to anomalous
259 high-pressure behavior, as discussed in Zucchini et al. (2014). A detailed discussion is beyond the aim of this
260 work; however, we also noticed, and in agreement with Zucchini et al. (2014), a lack or a shift towards high
261 pressure of the dolomite to dolomite-II transition in disordered dolomite when compared to *R*-3 dolomite.
262 Fe-dolomite presents a similar bulk modulus (*i.e.,* K_0=93(1) GPa) to dolomite.

263 Samples in the magnesite-siderite join have a compressional behavior that is described by a 2nd order BM
264 EoS. The bulk modulus is reasonably higher than Ca-bearing carbonates, and increase from magnesite to
265 siderite (Fig. 5a). The measured values agree with literature data (*i.e.*, Fiquet et al. 1994; Ross et al. 1997;
266 Lavina et al. 2010b; Lin et al. 2013; Litasov et al. 2013). A linear regression curve indicates a bulk modulus
267 K_0=122.7 (GPa) for pure siderite. The scattering of these experimental data are likely related to the deviation
268 for pure magnesite-siderite join, due do the presence of minor Mn and Ca content. From these data we may
269 extrapolate the bulk modulus of 118 GPa for a sample with a composition $Mg_{0.6}Fe_{0.4}CO_3$. This value is useful

to compare the bulk modulus variation over calcite-magnesite and calcite-Fe-magnesite joins (Fig. 5b). We observe that the bulk modulus increases from calcite to magnesite, and from calcite to Fe-magnesite, with an almost linear trend. The presence of Fe increases the bulk modulus; this is most noticeable along the magnesite-siderite join.

Discussion and implications

Despite the large amount of experimental data acquired and published in the recent years, the effect of Fe in thermal and elastic properties of carbonates was unconstrained, with the exception of a recent paper on siderite (Litasov et al. 2013) based on *in-situ P-V-T* data from energy-dispersive diffraction experiment. The high-temperature data show that thermal expansion decreases as Fe content increases in carbonates. This behavior is also observed in pyroxenes, ***e.g.*** Hugh-Jones (1997). The high-pressure behavior shows that the Fe-bearing samples are less compressible (*i.e.*, higher bulk moduli) than the Fe-free corresponding carbonates. These data are important for the thermodynamic modelling of Fe-carbonates at high temperatures (*e.g.*, Kang et al. 2015). The data reported for Fe-free carbonates are comparable to the most accurate data in literature. The *V-P* and *T-V* equation of state here reported are useful in modelling the volume behavior of carbonates at variable pressures and temperature. We here compare the calculated volume of dolomite and Fe-dolomite as a function of pressures and temperatures, with experimental data, based on two *in-situ* experiments. The computed volumes are based on *P-V* and *V-T* EoS, assuming the derivative of bulk modulus with temperature, $\partial K/\partial T$ = -0.02, a value which can approximate the behavior of mantle minerals (*e.g.*, Shim et al. 2000; Angel et al. 2014). The experimental volume of dolomite and Fe-dolomite is based on monochromatic X-ray powder diffraction experiments performed with a multianvil press and synchrotron radiation. An example of the high-resolution X-ray powder pattern is reported in Fig. 6. The data are fitted by the Rietveld method. About twenty X-ray diffraction patterns were collected for dolomite and Fe-dolomite at variable pressures and temperatures. The measured volume is compared with the calculated one at the corresponding pressure and temperature and the difference is plotted in Fig. 7 (as function of temperature). The numerical data are reported in the Deposit Items. For comparison, the volume difference

296 calculated using the EoS parameters of calcite and magnesite are also reported. The ordered/disordered
297 configuration in dolomite does not affect significantly the volume behavior, at least as a first approximation
298 and within the experimental accuracy achieved in these experiments. We noticed the disappearance of
299 superstructure peaks of the ordered configuration at high temperature, without volume discontinuity, in
300 agreement with previous determined temperatures (Hammouda et al. 2011; Franzolin et al. 2012). The
301 minimum discrepancies between measured and calculated volume data indicates that the reported EoS
302 parameters and the current experimental accuracy in monochromatic *in-situ* experiments, may provide the
303 needed accuracy and precision for planning *in-situ* kinetic experiments, where change of composition of
304 carbonates is expected, especially concerning the variation of Ca/(Mg+Fe) ratio. This is the case, for
305 example, during exsolution and incongruent melting of carbonates (*e.g.*, Franzolin et al., 2011), whose
306 relations are still not known completely, and especially, in the subsolidus relations of calcite-Fe-magnesite
307 system, with direct application to the understanding of carbonate stability in subduction environments. The
308 quantitative knowledge of such phenomena may, in fact, provide fundamental insights to understand the
309 major geological processes involving carbon exchange between the different reservoirs in the Earth's upper
310 mantle.

311

312 # Acknowledgments

313 We acknowledge Andrea Risplendente and Nicola Rotiroti for the assistance in the microprobe analysis and
314 single crystal laboratory diffraction. We acknowledge Elettra Syncrotron Facility for provision of beamtime
315 (experiment 20125293, 20135433). We acknowledge ESRF for provision of beamtime (experiment ES142,
316 ES209). MM acknowledge DCO support.

317

318

References

Angel, R. J., Alvaro, M., and Gonzalez-Platas, J. (2014) EosFit7c and a Fortran module (library) for equation of state calculations. Zeitschrift für Kristallographie-Crystalline Materials, 229, 405-419.

Angel, R.J. (2000) High-pressure, high-temperature crystal chemistry. In R.M. Hazen and R.T. Downs, Eds., High-Temperature and High-Pressure Crystal Chemistry, 41, p. 35–59. Reviews in Mineralogy and Geochemistry, Mineralogical of Society America, Chantilly, Virginia.

Antao, S. M., Hassan, I., Mulder, W. H., Lee, P. L. and Toby, B. H. (2009) In situ study of the R-3c to R-3m orientational disorder in calcite. Phys. Chem. Minerals 36, 159–169.

Berg, G.W. (1986) Evidence for carbonate in the mantle. Nature, 324, 50-51.

Boulard, E., Guyot, F. and Fiquet, G. (2012) The influence on Fe content on Raman spectra and unit cell parameters of magnesite–siderite solid solutions. Physics and chemistry of minerals, 39, 239-246.

Busing, W., and Levy, H.A. (1967) Angle Calculations for 3- and 4- Circle X-ray and Neutron Diffractometers. Acta Crystallographica, 22, 457-464.

Colonna, F., Fasolino. A. and Meijer, E.J. (2011) High-pressure high-temperature equation of state of graphite from Monte Carlo simulations. Carbon, 49, 364-368.

Datchi, F., LeToullec, R., and Loubeyre, P. (1997) Improved calibration of the SrB_4O_7: Sm^{2+} optical pressure gauge: Advantages at very high pressures and high temperatures. Journal of applied physics 81, 3333-3339.

Dewaele A., Fiquet G., Andrault D., and Hausermann D. (2000) P-V-T equation of state of periclase from synchrotron radiation measurements. Journal of geophysical research, 105, 2869-2877.

Dove, M. T., and Powell, B. M.(1989) Neutron diffraction study of the tricritical orientational order/disorder phase transition in calcite at 1260 K. Physics and Chemistry of Minerals 16, 503–507.

Dove, M. T., Swainson, I. P., Powell, B. M. and Tennant, D. C. (2005) Neutron powder diffraction study of the orientational order–disorder phase transition in calcite, CaCO3. Physics and Chemistry of Minerals 32, 493–503.

Effenberger, H., Mereiter, K., and Zemann, J. (1981) Crystal structure refinements of magnesite, calcite, rhodochrosite, siderite, smithonite, and dolomite, with discussion of some aspects of the stereochemistry of calcite type carbonates. Zeitschrift für Kristallographie, 156, 233–243.

Fei, Y. (1995) Thermal expansion. In Ahrens, T.J. (ed) Mineral Physics and Crystallography, A Handbook of Physical Constants. Am Geophys Union, Washington, DC

Fiquet, G., Guyot, F. and Itie, J.-P. (1994) High-pressure X-ray diffraction study of carbonates: MgCO3, CaMg(CO3)2, and CaCO3. American Mineralogist, 79, 15-23.

Fiquet, G., Guyot, F., Kunz, M., Matas, J., Andrault, D., and Hanfland, M. (2002) Structural refinements of magnesite at very high pressure. American Mineralogist, 87, 1261–1265.

Forman, R.A., Piermarini, G.J., Barnett, J.D., and Block, S. (1972) Pressure measurement made by the utilization of ruby sharp-line luminescence. Science, 176, 284-285.

Franzolin E., Merlini M., Poli S., Schmidt M.W. (2012) The temperature and compositional dependence of disordering in Fe-bearing dolomites. American Mineralogist, 97, 1676-1684.

Franzolin, E., Schmidt, M.W., Poli S. (2011) Ternary Ca–Fe–Mg carbonates: subsolidus phase relations at 3.5 GPa and a thermodynamic solid solution model including order/disorder. Contribution to Mineralogy and Petrology, 161, 213-227.

Hammouda, T., Andrault, D., Koga, K., Katsura, T., Martin, A.M. (2011) Ordering in double carbonates and implications for processes at subduction zones. Contribution to Mineralogy and Petrology, 161, 439-450.

Hanfland M., Syassen, K., and Sonnenschein, R. (1989) Graphite under pressure – Equation of state and 1st-order Raman modes. Physical Review B, 40, 1951-1954.

Hazen R.M. (1976) Effects of temperature and pressure on the cell dimension and X-ray temperature factors of periclase. American Mineralogist, 61, 266-271.

Holland T.J.B., and Powell R. (1998) An internally consistent thermodynamic data set for phases of petrological interest. Journal of metamorphic geology, 16, 309-343

Holland, T. J. B., and Powell, R. (2011) An improved and extended internally consistent thermodynamic dataset for phases of petrological interest, involving a new equation of state for solids. Journal of Metamorphic Geology, 29, 333-383.

Hugh-Jones, D. (1997) Thermal expansion of MgSiO3 and FeSiO3 ortho- and clinopyroxenes. American Mineralogist, 82, 689–696.

Ishizawa N., Setoguchi H., and Yanagisawa K. (2013) Structural evolution of calcite at high temperatures: Phase V unveiled. Scientific reports 3, 2832.

Kang, N., Schmidt M.W., Poli, S., Franzolin E., and Connolly, J.D. (2015) Melting of siderite to 20 GPa and thermodynamic properties of FeCO3-melt. Chemical Geology, 400, 34–43.

Kihara K, (1990) An X-ray study of the temperature dependence of the quartz structure. European Journal of mineralogy, 2, 63-77.

Larson A.C. and Von Dreele R.B. (1994) General Structure Analysis System (GSAS), Los Alamos National Laboratory Report LAUR 86-748.

Lavina, B., Dera, P., Downs, R.T., Tschauner, O., Yang, W.E., Shebanova, O., and Shen, G.Y. (2010b) Effect of dilution on the spin pairing transition in rhombohedral carbonates. High Pressure Research, 30, 224–229.

Lavina, B., Dera, P., Downs, R.T., Yang, W.G., Sinogeikin, S., Meng, Y., Shen, G.Y., and Schiferl, D. (2010a) Structure of siderite FeCO3 to 56 GPa and hysteresis of its spin-pairing transition. Physical Review B, 82, 064110.

Lin, J.F., Liu, J., Jacobs, C., and Prakapenka, V.B. (2012) Vibrational and elastic properties of ferromagnesite across the electronic spin-pairing transition of iron. American Mineralogist, 97, 583–591.

Litasov K.D., Shatskiy A., Gavryushkin P.N., Sharygin I.S., Dorogokupets P.I., Dymshits A.M., Ohtani E., Higo Y., and Funakoshi K. (2013) P–V–T equation of state of siderite to 33 GPa and 1673 K. Physics of the Earth and Planetary Interiors 224 (2013) 83–87.

Mao, H.K., Xu, J., and Bell, P.M. (1986) Calibration of the Ruby Pressure Gauge to 800 kbar Under Quasi-

395 Hydrostatic Conditions. Journal of Geophysical Research, 91, 4673-4676.

396 Mao, Z., Armentrout, M., Rainey, E.S.G., Manning C.E., Dera, P., Prakapenka, V., and Kavner, A. (2011)
397 Dolomite III: A new candidate lower mantle carbonate. Geophysical Research Letters, 38, L22303.

398 Markgraf, S. A. and Reeder, R. J. (1985) High-temperature structure refinements of calcite and magnesite.
399 American Mineralogist 70, 590–600.

400 Markgraf, S. A. and Reeder, R. J. (1985) High-temperature crystal chemistry of dolomite. American
401 Mineralogist 71, 795–804.

402 Mattila, A., Pylkkanen, T., Rueff, J.P., Huotari, S., Vanko, G., Hanfland, M., Lehtinen, M., and Hamalainen,
403 K. (2007) Pressure induced magnetic transition in siderite FeCO3 studied by X-ray emission
404 spectroscopy. Journal of Physics-Condensed Matter, 19, 386206

405 Merlini, M., and Hanfland, M. (2013) Single-crystal diffraction at megabar conditions by synchrotron
406 radiation. High Pressure Research, 33, 511-522.

407 Merlini, M., Crichton, W., Hanfland, M., Gemmi, M., Müller, H., Kupenko, I., and Dubrovinsky, L. (2012)
408 Structures of dolomite at ultrahigh pressure and their influence on the deep carbon cycle,
409 Proceedings of the National Academy of Sciences of the U.S. A., 109, 13509-13514.

410 Merrill, L. and Bassett, W.A. (1975) The crystal structure of CaCO3(II), a high-pressure metastable phase of
411 calcium carbonate. Acta Crystallographica B, 31, 343-349.

412 Miletich, R., Gatta, G.D., Willi, T., Mirwrwald, P.W., Lotti, P., Merlini, M., Rotiroti, N. and Loerting, T.
413 (2014) Cordierite under hydrostatic compression: Anomalous elastic behavior as a precursor for a
414 pressure-induced phase transition. American Mineralogist, 99, 479–493.

415 Mirwald, P. W. (1976) A differential thermal analysis study of the high-temperature polymorphism of
416 calcite at high pressure. Contribution to Mineralogy and Petrology 59, 33–40.

417 Navon, O. (1999) Diamond formation in the Earth's mantle. In J.J. Gurney, J.L. Gurney, M.D. Pascoe, and
418 S.H. Richardson, Eds., VII International Kimberlite conference 2, 584–604. Red Roof Design, Cape
419 Town.

Oganov A.R., Hemley, R.J., Hazen, R.M. and Jones, A.P. (2013) Structure, bonding, and mineralogy of carbon at extreme conditions, in: R.M. Hazen, A.P. Jones, J.A. Baross (Eds.), Carbon in Earth, 75, 47-77. Reviews in Mineralogy and Geochemistry, Mineralogical Society of America, Washington, U.S.A.

Oxford Diffraction (2008) Crysalis RED, Version 1.171.32.29.

Pawley, A.R., Redfern, S.A.T., and Holland, J.B. (1996) Volume behavior of hydrous minerals at high pressure and temperature: I. Thermal expansion of lawsonite, zoisite, clinozoisite, and diaspore. American Mineralogist, 81, 335-340.

Petříček, V., Dušek, M., and Palatinus, L. (2014) Crystallographic Computing System JANA2006: General features. Zeitschrift für Kristallographie-Crystalline Materials, 229, 345-352.

Rao K.V.K., Naidu S.V.N., and Murthy K.S. (1968) Precision lattice parameters and thermal expansion of calcite. Journal of Physics and Chemistry of Solids, 29, 245-248.

Rebuffi L, Plaisier JR, Abdellatief M, Lausi A, and Scardi P (2014) MCX: A synchrotron radiation beamline for X-ray diffraction line profile analysis. Zeitschrift fur Anorganische und Allgemeine Chemie 640, 3100-3106.

Redfern, S.A.J., Salji, E., and Navtrotsky, A. (1989) High-temperature enthalpy at the orientational order/disorder transition in calcite: Implications of the calcite/aragonite phase equilibrium. Contributions to Mineralogy and Petrology, 101,479–484.

Redfern, S.A.T. (2000) Structural variations in carbonates. In R.M. Hazen and R.T. Downs, (eds.), High-Temperature and High-Pressure Crystal Chemistry, 41, 289–308. Reviews in Mineralogy and Geochemistry, Mineralogical Society of America, Washington, U.S.A.

Redfern, S.A.T., and Angel, R.J. (1999) High-pressure behaviour and equation of state of calcite, CaCO3. Contributions to Mineralogy and Petrology. 134,102-106.

Redfern, S.A.T. (2000) Structural variations in carbonates. Reviews in Mineralogy and Geochemistry, 41, 289–308.

Reeeder, R.J. (1983) Crystal chemistry of the rhombohedral carbonates In R J. Reeder, Ed., Carbonates:

446 Mineralogy and chemistry. Mineralogical Society of America Reviews in Mineralogy, 11,147.

447 Reeder, R.J., and Dollase, W.A. (1989) Structural variation in the dolomite-ankerite solid-solution series; an
448 X-ray, Mössbauer, and TEM study. American Mineralogist, 74, 1159–1167.

449 Riello P, Lausi A, MacLeod J, Plaisier JR, Zerauschek G, and Fornasiero P (2013). In situ reaction furnace
450 for real-time XRD studies. Journal of Synchrotron Radiation, 20, 194-196.

451 Ross, N. (1997) The equation of state and high-pressure behavior of magnesite. American Mineralogist, 82,
452 682–688.

453 Ross, N.L., and Reeder, R.J. (1992) High-pressure structural study of dolomite and ankerite. American
454 Mineralogist, 77, 412-421.

455 Santillan, J., Williams, Q., and Knittle, E. (2003) A high-pressure polymorph of CaMg(CO3)2.Geophysical
456 Research Letters, 30,1054.

457 Shim S.H., and Duffy, T.S. (2000). Constraints on the P-V-T equation of state of $MgSiO_3$ perovskite.
458 American Mineralogist, 85, 354-363.

459 Toby B. H. (2001) EXPGUI, a graphical user interface for GSAS, J. Appl. Cryst. 34, 210-213.

460 Zucchini, A., Comodi, P., Nazzareni, S., and Hanfland, M. (2014) The effect of cation ordering and
461 temperature on the high-pressure behaviour of dolomite. Physics and Chemistry of Minerals, 41,
462 783-793.

463

This is a preprint, the final version is subject to change, of the American Mineralogist (MSA)
Cite as Authors (Year) Title. American Mineralogist, in press.
(DOI will not work until issue is live.) DOI: http://dx.doi.org/10.2138/am-2016-5458

Tables

Sample	Locality	Composition	Crystallographic data	Experiment
Calcite	Esztramos Hill (Hungary)	$CaCO_3$	*a*=4.9902(2), *c*=17.0631(9), *V*=367.98(3)	SC, HT
Mg-Fe-calcite	Synthetic	$(Ca_{0.96}Mg_{0.02}Fe_{0.01})CO_3$	*a*=4.9755(2), *c*= 17.0053(17), *V*=364.58(7)	SC
Mg-Fe-Calcite	Synthetic	$(Ca_{0.91}Mg_{0.06}Fe_{0.03})CO_3$	*a*=4.9462(7), *c*=16.881(3), *V*=357.66(16)	SC, HT, HP
Ca-Dolomite (disordered)	Synthetic	$(Ca_{0.55}Mg_{0.45})CO_3$	*a*=4.8337(3), *c*=16.2329(12), *V*=328.46(3)	SC, HP
Dolomite	Bazena (Italy)	$CaMg(CO_3)_2$	*a*=4.8091(1), *c*=16.020(1), *V*=320.86(11)	SC, HT, HP, HT/HP
Fe-dolomite	Col du Petit San Bernard (France/Italy)	$Ca_{1.01}Mg_{0.9}Fe_{0.08}Mn_{0.01}(CO_3)_2$	*a*=4.8108(3), *c*=16.0412(8), *V*=321.51(10)	SC
Fe-dolomite	La Mure (France)	$Ca(Mg_{0.6}Fe_{0.4})(CO_3)_2$	*a*=4.8189(2), *c*=16.0912(7), *V*=323.60(2)	SC, HT, HP, HT/HP
Magnesite	Val Solda	$(Mg_{0.99}Fe_{0.01})CO3$	*a*=4.6348(19), *c*=15.0235(8), *V*=279.49(3)	SC, HP
Magnesite	Czechoslovakia	$(Mg_{0.99}Fe_{0.01})CO3$	*a*=4.6371(2), *c*= 15.0365(13), *V*=280.01(5)	SC, HT
Fe-Magnesite	Tyrol (Austria)	$Mg_{0.89}Fe_{0.11}(CO_3)$	*a*=4.64475(17), *c*=15.0805(6), *V*=281.754(14)	SC, HT, HP
Siderite	Puits de Villaret (France)	$(Fe_{0.70}Mg_{0.26}Mn_{0.025}Ca_{0.015})CO_3$	*a*=4.6836(2), *c*=15.3177(14), *V*=290.99(2)	SC, HT, HP
Siderite	Foppolo (Italy)	$(Fe_{0.74}Mg_{0.21}Mn_{0.04}Ca_{0.01})CO_3$	*a*=4.6875(3), *c*=15.3547(9), *V*=292.19(3)	SC, HP
Siderite	Ivigtut (Greenland)	$(Fe_{0.95}Mn_{0.045}Mg_{0.005})CO_3$	*a*=4.6924(2), *c*=15.3865(9), *V*=293.39(2)	SC, HT, HP

Table 1 – Samples used in the current study for the single crystal (SC) diffraction experiments at ambient conditions, high-temperature (H*T*) X-ray powder diffraction experiments and high-pressure (H*P*) single crystal X-ray diffraction. The compositions were determined by electron microprobe analysis. Axial unit-cell parameters in Å, unit-cell volume in $Å^3$.

	Fit Pawley, 1 term		Fit Fei, 2 terms		
Sample	V_0 ($Å^3$)	a_0 (K^{-1})*10^5	V_0 ($Å^3$)	a_0 (K^{-1}) *10^5	a_1 (K^{-2})*10^8
calcite Hungary	366.70(5)	4.10(7)	366.80(4)	0.27(6)	3.59(11)
$(Ca_{0.91}Mg_{0.06}Fe_{0.03})CO_3$ syn	355.92(8)	5.64(9)	356.10(10)	1.3(3)	3.0(5)
dolomite Bazena	321.00(1)	6.40(2)	321.00(2)	2.20(9)	2.46(15)
Fe-dolomite La Mure	323.50(14)	6.33(3)	323.50(2)	2.05(14)	2.7(2)
magnesite Czech	280.20(1)	7.04(2)	280.10(1)	2.62(9)	2.39(16)
Fe-magnesite Tyrol	280.87(1)	7.01(5)	280.90(1)	1.8(3)	4.2(7)
siderite Puits de Villaret	290.60(1)	6.51(3)	290.60(1)	2.05(14)	3.0(3)
siderite Ivigtut	293.40(11)	6.44(5)	293.30(1)	2.48(7)	1.97(14)

Table 2 – Results of fitting procedure on high-temperature volume data, using the Pawley et al. (1996) formalism with one thermal expansion coefficient (eq. 5), and Fei (1995) formalism (eq. 7) with two thermal expansion coefficients. Additional results using the Pawley expression with two coefficients and a linear expression are in the Deposit Items.

480

sample	V_0 (Å^3)	K_0 (GPa)	K'
$(Ca_{0.91}Mg_{0.06}Fe_{0.03})CO_{3\ syn}$	360.5(1)	77(3)	-3.8(17)
$(Ca_{0.55}Mg_{0.45})CO_3$	329.1(4)	89(2)	3.0(2)
dolomite Bazena	320.7(3)	94(1)	4
Fe-dolomite La Mure	321.1(4)	93(1)	4
magnesite Czech	279.0(5)	113(1)	4
Fe-magnesite Tyrol	280.9(2)	115.9(9)	4
siderite Puits de Villaret	288.0(4)	123(1)	4
siderite Foppolo	291.0(8)	125(2)	4
siderite Ivigtut	293.4(2)	117.7(9)	4

481

482 Table 3 – Elastic parameters of carbonates (by BM EoS fit) in the ternary diagram.

483

484

485

486

Figures

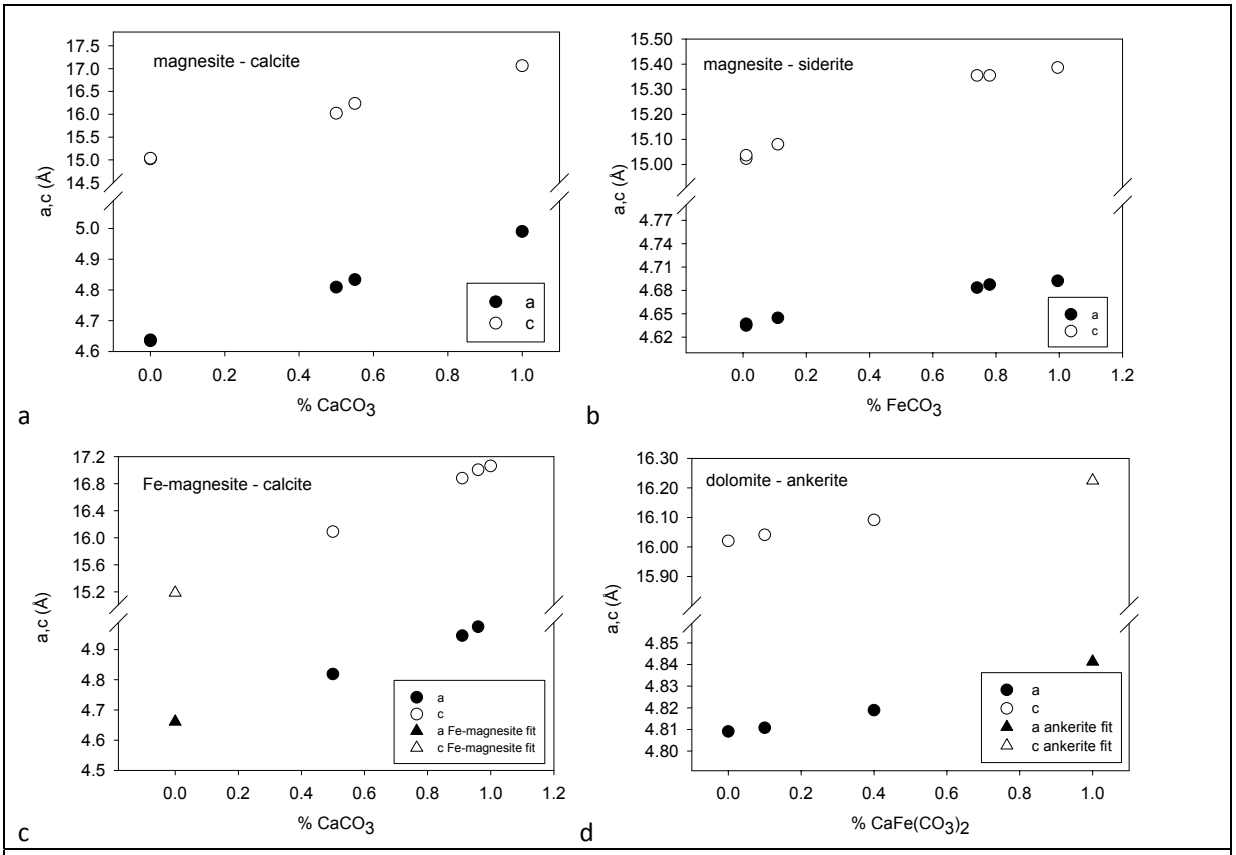

Fig. 1 – Unit-cell parameters as function of composition for (a) magnesite-calcite; (b) magnesite-siderite; (c) Fe-magnesite-calcite; d) dolomite-ankerite joins. The circles refer to experimental data. The triangles are derived from a fit of the available points. The error bars have a comparable size with the symbols.

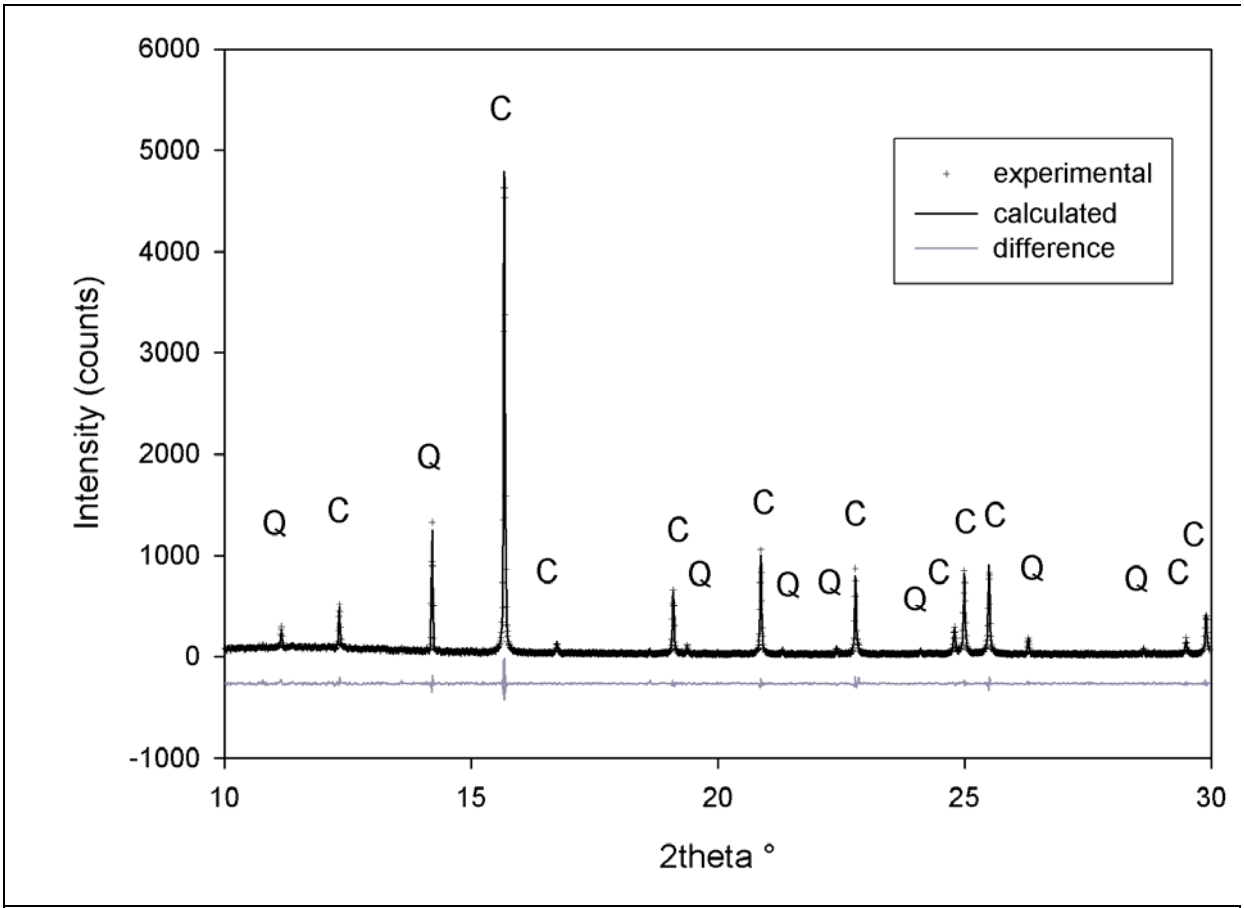

Fig. 2 – X-ray powder diffraction pattern of the mixture calcite (C) +quartz (Q) used at ambient conditions. The Rietveld full-profile fit and the difference curve are shown.

491

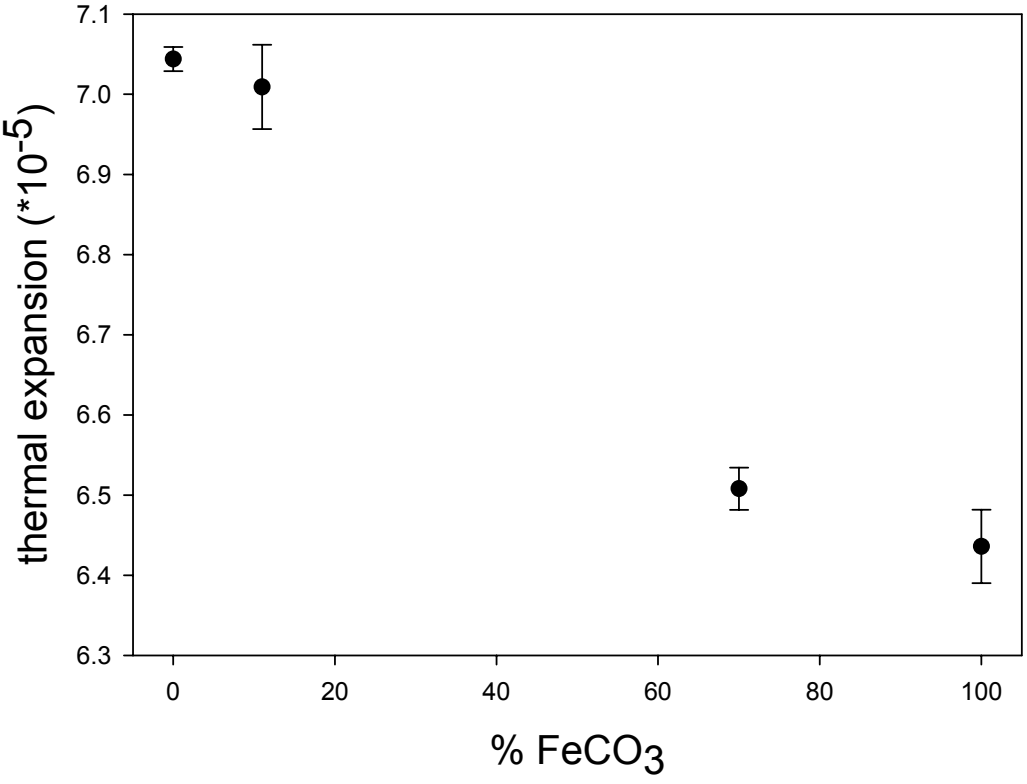

Fig. 3 – Thermal expansion coefficient (a_0, cf. eq. 5) in the magnesite-siderite binary join

492

493

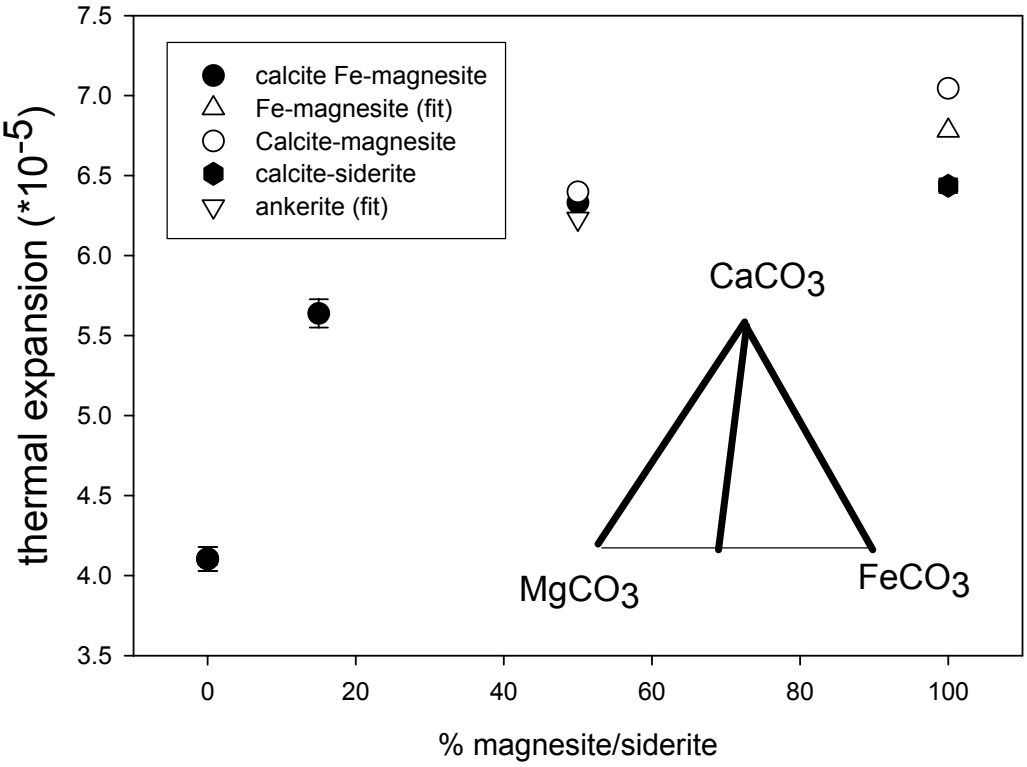

Fig. 4 – Thermal expansion coefficients in the binary compositional joins $CaCO_3$-$MgCO_3$, $CaCO_3$-$(Mg,Fe)CO_3$, $CaCO_3$-$FeCO_3$.

494

495

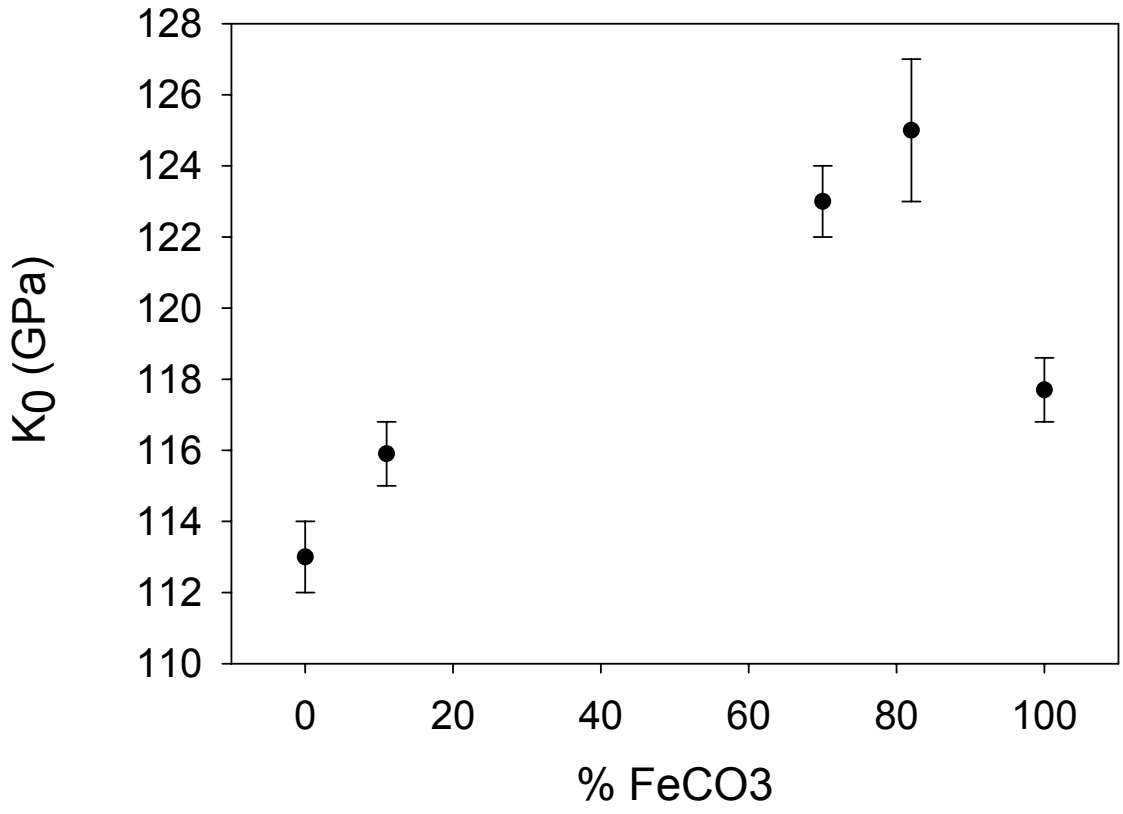

496

497 Fig. 5a – Bulk moduli along the siderite-magnesite join.

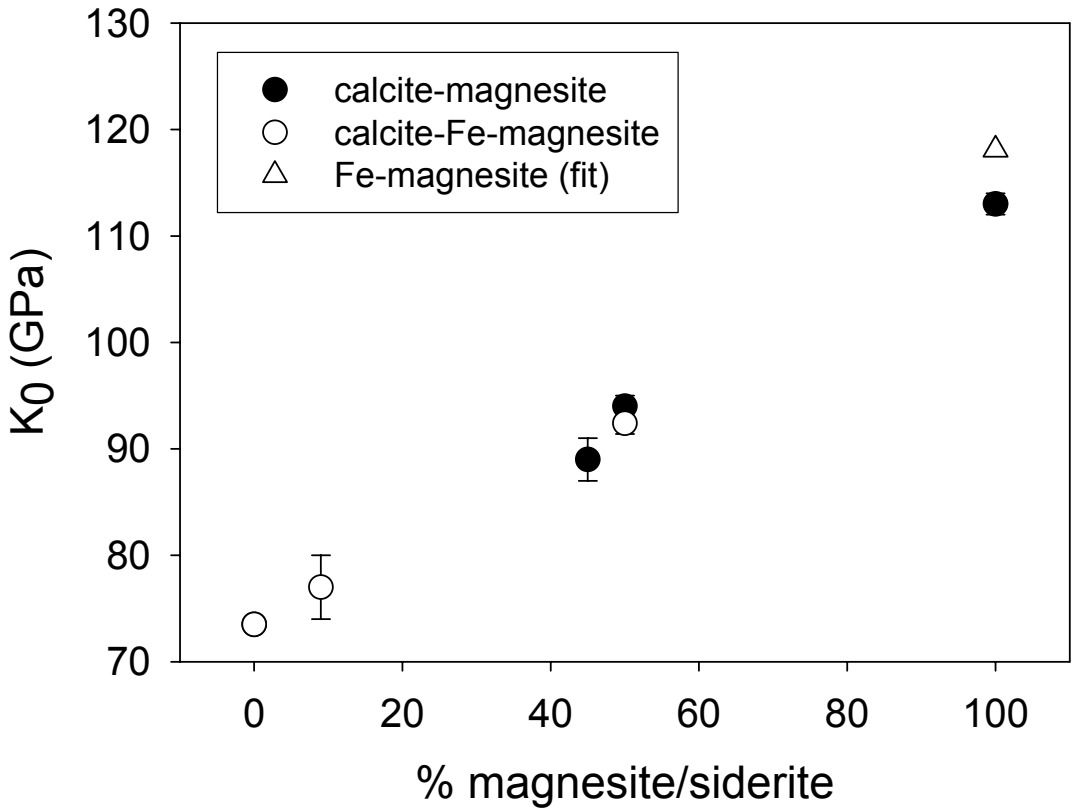

498

499 Figure 5b. Bulk moduli along the calcite-magnesite and calcite-Fe-magnesite binary joins.

500

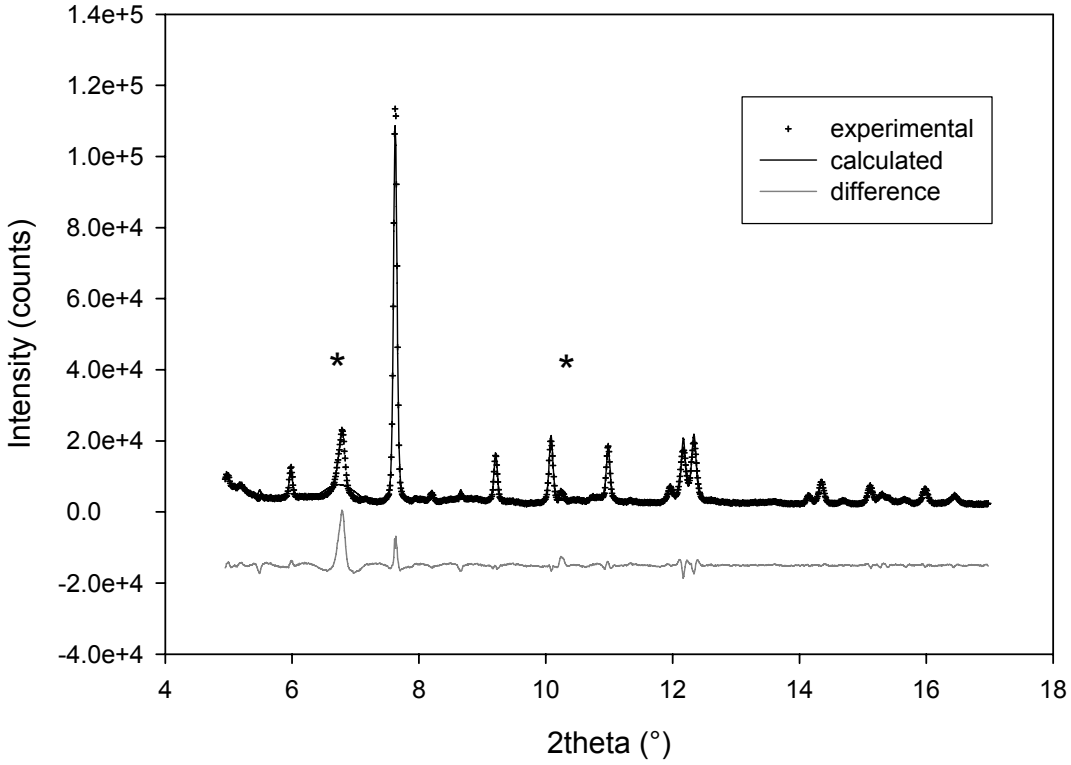

501

502 Fig. 6 – X-ray powder pattern of Fe-dolomite (cross) at high pressure and temperature, Rietveld full-profile
503 fit (black line) and difference curve (gray line). The diffraction peaks of graphite and MgO are marked with
504 asterisk.

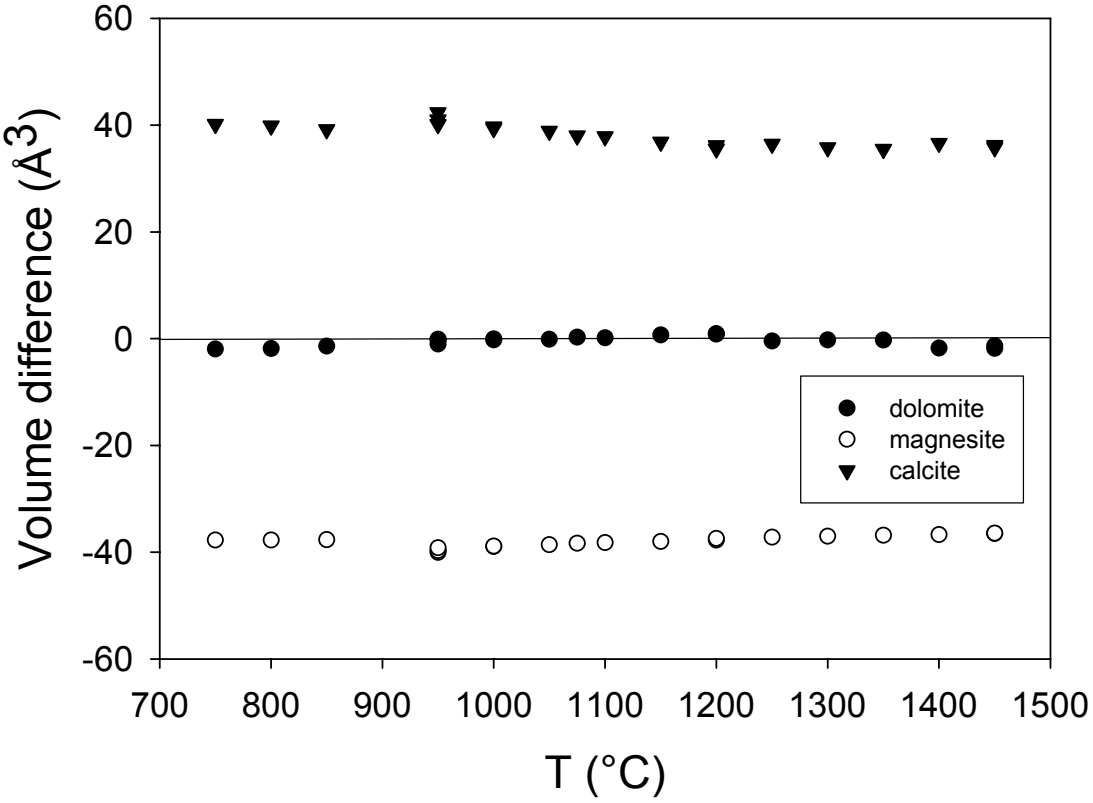

505

506 Fig 7a

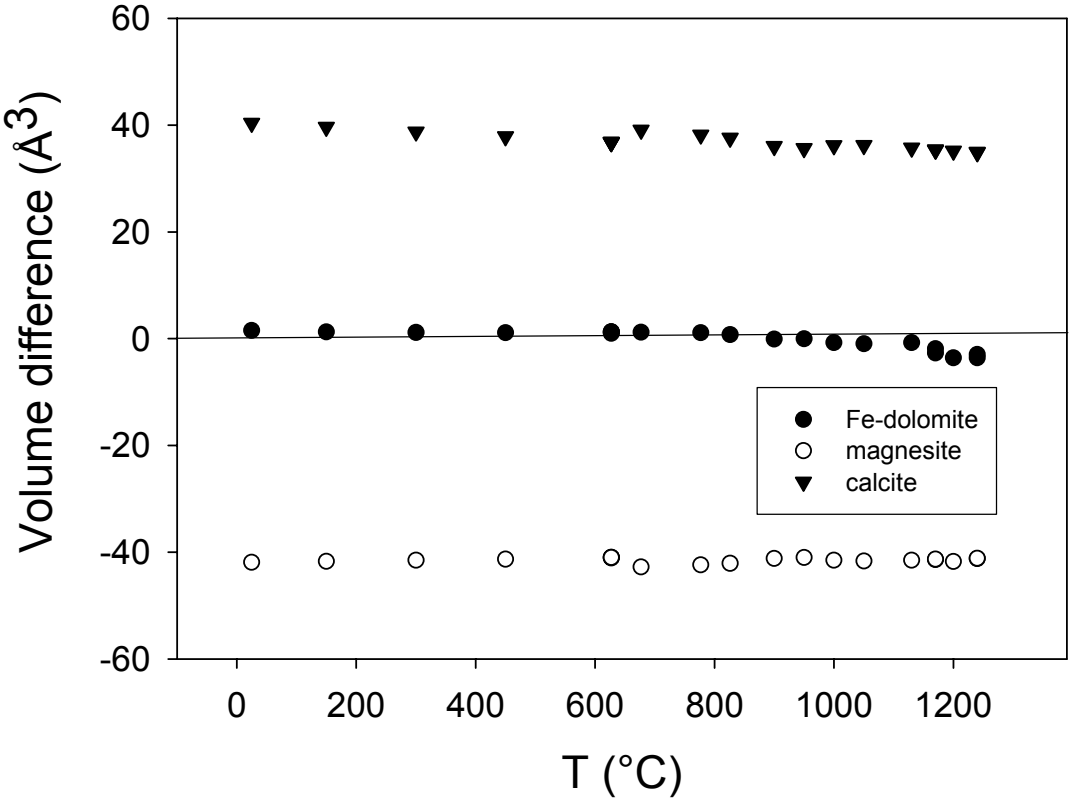

507

508 Fig. 7b

509

510

511 Figure 7 – Difference in calculated and experimental volume of dolomite (a) and Fe-dolomite (b). The
512 experimental and computed data refer to a series of *P* and *T* points (Deposit Items). All the points are
513 plotted using only temperature as variable. For comparison, also the volume difference with pure
514 calcite and magnesite are reported, with the data of calcite and magnesite computed from the EoS of
515 this paper at the corresponding *P* and *T*.